Structure of ^{55}Ti from relativistic one-neutron knockout

P. Maierbeck [a,*], R. Gernhäuser [a], R. Krücken [a], T. Kröll [a], H. Alvarez-Pol [b], F. Aksouh [c], T. Aumann [c], K. Behr [c], E.A. Benjamim [b], J. Benlliure [b], V. Bildstein [a], M. Böhmer [a], K. Boretzky [c], M.J.G. Borge [d], A. Brünle [c], A. Bürger [e,f], M. Caamaño [b], E. Casarejos [b], A. Chatillon [c], L.V. Chulkov [c], D. Cortina-Gil [b], J. Enders [g], K. Eppinger [a], T. Faestermann [a], J. Friese [a], L. Fabbietti [a], M. Gascón [b], H. Geissel [c], J. Gerl [c], M. Gorska [c], P.G. Hansen [h,1], B. Jonson [i], R. Kanungo [j,k,c], O. Kiselev [c,l,m], I. Kojouharov [c], A. Klimkiewicz [c], T. Kurtukian [b], N. Kurz [c], K. Larsson [c,i], T. Le Bleis [c,n], K. Mahata [c,o], L. Maier [a], T. Nilsson [i,g], C. Nociforo [c], G. Nyman [i], C. Pascual-Izarra [d], A. Perea [d], D. Perez [b], A. Prochazka [c,p], C. Rodriguez-Tajes [b], D. Rossi [l], H. Schaffner [c], G. Schrieder [g], S. Schwertel [a], H. Simon [c], B. Sitar [p], M. Stanoiu [c], K. Sümmerer [c], O. Tengblad [d], H. Weick [c], S. Winkler [a], B.A. Brown [h], T. Otsuka [q], J. Tostevin [r], W.D.M. Rae [s]

a Physik Department E12, Technische Universität München, 85748 Garching, Germany
b Departemento de Física de Partículas, Universidade de Santiago de Compstela, 15782 Santiago de Compostela, Spain
c GSI Helmholtzzentrum für Schwerionenforschung, 64291 Darmstadt, Germany
d Instituto de Estructura de la Materia, CSIC, 28006 Madrid, Spain
e SAFE/OCL, University of Oslo, N-0316 Oslo, Norway
f CEA, Saclay, DSM/IRFU/SPhN, F-91191 Gif-sur-Yvette, France
g Institut für Kernphysik, Technische Universität Darmstadt, 64289 Darmstadt, Germany
h NSCL, Michigan State University, East Lansing, MI 48824, USA
i Experimentell Fysik, Chalmers Tekniska Högskola och Göteborgs Universitet, 412 96 Göteborg, Sweden
j TRIUMF, 4004 Wesbrook Mall, Vancouver, British Columbia V6T 2A3, Canada
k Saint Mary's University, 923 Robie St., Halifax, Nova Scotia B3H 3C3, Canada
l Johannes Gutenberg Universität, 55099 Mainz, Germany
m Paul Scherrer Institut, 5232 Villigen, Switzerland
n Institut Pluridisciplinaire Hubert Curien IN2P3-CNRS/Université Louis Pasteur, F-67037 Strasbourg Cedex 2, France
o Nuclear Physics Division, Bhabha Atomic Research Centre, Mumbai 400 085, India
p Faculty of Mathematics and Physics, Comenius University, 84215 Bratislava, Slovakia
q Department of Physics, University of Tokyo, Hongo, Bunkyo-ku, Tokyo 113-0033, Japan
r Department of Physics, Faculty of Engineering and Physical Sciences, University of Surrey, Guildford, Surrey GU2 7XH, United Kingdom
s Garsington, Oxfordshire, OX44, United Kingdom

A R T I C L E   I N F O

A B S T R A C T

Results are presented from a one-neutron knockout reaction at relativistic energies on ^{56}Ti using the GSI FRS as a two-stage magnetic spectrometer and the MINIBALL array for gamma-ray detection. Inclusive and exclusive longitudinal momentum distributions and cross-sections were measured enabling the determination of the orbital angular momentum of the populated states. First-time observation of the 955(6) keV $\nu p_{3/2}^{-1}$-hole state in ^{55}Ti is reported. The measured data for the first time proves that the ground state of ^{55}Ti is a $1/2^-$ state, in agreement with shell-model calculations using the GXPF1A interaction that predict a sizable $N = 34$ gap in ^{54}Ca.

1. Introduction

One of the most interesting topics in modern nuclear structure research is the evolution of shell structure in nuclei far from the

* Corresponding author. Tel.: +49 89 28912488; fax: +49 89 28912297.
E-mail address: peter.maierbeck@physik.tu-muenchen.de (P. Maierbeck).
1 Deceased.

valley of stability. Modifications of the well-established shell structure at stability may be expected for exotic nuclei due to evolution of the mean field itself, e.g. through changes of the spin–orbit interaction or the residual interaction. The local modification of shell structure due to the effects of the residual interaction among the valence nucleons has been the subject of many theoretical and experimental studies in recent years (see, e.g., [1] for a recent review). It has been found that the monopole part of the tensor force may play an important role in such shell-structure modifications [2–4]. However, the role of the tensor force and the strength of the spin–orbit term may ultimately turn out to be linked (see e.g. [5]).

The region of neutron-rich Ca, Ti, and Cr nuclides around $N = 32, 34$ is of particular recent interest. Theoretical predictions based on shell-model calculations, using a new interaction (GXPF1, GXPF1A) for the fp-shell [6], predict a new doubly-magic shell closure for the $N = 34$ nucleus ^{54}Ca. At the same time, shell-model calculations using the well established KB3G interaction [7–10], and results from beyond mean-field theory using the D1S parametrization of the Gogny force [11] support an $N = 32$ but not an $N = 34$ shell closure.

While the central nucleus in this region, ^{54}Ca, cannot be reached experimentally yet, it is important to map the region close to the predicted new shell closures. A number of studies have been performed on neutron rich $Z = 20–24$ nuclei using β-decay [12–16], multi-nucleon transfer in deep-inelastic collisions [14,17–19], Coulomb excitation of radioactive ion beams [20,21], and knockout reactions [22,23]. In particular, it has recently been possible to observe excited states in ^{55}Ti via multi-nucleon transfer [19]. The level scheme obtained compares favorably with shell-model calculations using the GXPF1A interaction and tentative spin assignments were made on the basis of these calculations.

This Letter reports on the results of a single-neutron knockout experiment at relativistic energy using a secondary beam of ^{56}Ti. While there were already Coulomb dissociation experiments in the region of ^{132}Sn [24,25] and ^{68}Ni [26], this is the first time that knockout experiments for medium-mass nuclei ($A \approx 50$) have been performed at relativistic energies, where the assumptions underlying the eikonal reaction theory used to analyse the experimental data are particularly well fulfilled.

2. Experimental details

The experiment was performed at the fragment separator (FRS) of GSI [27], Darmstadt, which was used as a two-stage spectrometer. Each stage comprised two 30° dipoles, scintillation counters for time-of-flight (TOF) as well as multiple-sampling ionization chambers (MUSIC) for energy-loss measurements. For the main experiment, a 500A MeV ^{86}Kr primary beam with an intensity of up to 10^9 particles per second was fragmented in a 1625 mg/cm^2 ^{9}Be production target at the entrance of the FRS. The fragments of interest were identified on an event-by-event basis and transported to the intermediate focal plane (S2) of the FRS, where they impinged on a ^{9}Be secondary reaction target of 1720 mg/cm^2 thickness for the knockout reactions. The reaction products of interest where identified event-by-event in the second dipole stage of the FRS and transported to the final FRS focus (S4). Mass and charge resolutions (FWHM) of $\Delta A = 0.1$ and $\Delta Z = 0.22$ were obtained, respectively.

Six time projection chambers (TPC), two before and two after the secondary target at S2 and two at S4, provided position and incident as well as emergent angles of primary fragments and reaction residues, respectively, allowing to reconstruct the flight path through the experimental setup. This enabled a precise measurement of the longitudinal momentum distributions of the heavy residues coming from the knockout reaction with a relative momentum resolution of 2×10^{-3} (FWHM). The FRS was operated

in the energy-loss mode. In this mode, the dispersion of the first spectrometer stage is matched to the dispersion of the second one. An energy (momentum) change due to the knockout reaction in the target can be measured with the second stage, independently of the energy (momentum) spread of the primary fragment.

Prompt gamma-rays emitted by the reaction products were detected with the eight triple-cluster detectors of the MINIBALL gamma-ray spectrometer [28]. These were arranged in a ring with an average distance of 26.4 cm between the front face of the detector and the center of the target and at an average azimuthal angle of 40° with respect to the beam axis. The absolute photopeak efficiency in the laboratory frame was determined to be 3.1% at 344.3 keV and 1.5% at 1332 keV. Using the 6-fold segmentation of the MINIBALL HPGe crystals for the Doppler correction of the gamma-rays, a resolution of $\approx$40 keV (FWHM) at a c.m. gamma-ray energy of about 580 keV was achieved for the relativistic velocities of the reaction products of $\beta \approx 0.7$, corresponding to a Lorentz factor of $\gamma \approx 1.54$. This resolution was limited by the solid angle of the detector segments.

A reference experiment was performed with a ^{48}Ca primary beam of 450A MeV impinging directly on the secondary target. The energy was chosen such that it corresponded to the energy of the primary fragments in the main experiment with the ^{86}Kr beam. The reaction ^{48}Ca $\rightarrow$ ^{47}Ca was used for the calibration of the set-up and to verify the analysis methods. For the analysis, a special database software was used [29]. Details of the analysis procedures are discussed in Ref. [30], while some results are summarized below.

In an 8.5 day experiment, in which the FRS was centered on ^{56}Ti in its first and ^{55}Ti in its second half, a total of 1.6×10^6 fully stripped ^{56}Ti primary fragments were detected. These led to the identification of 1.3×10^4 ^{55}Ti residues from the ^{56}Ti $\rightarrow$ ^{55}Ti knockout reaction. Fig. 1 shows on the left an identification plot of charge vs. mass-to-charge ratio at the FRS middle focus S2 before the knockout target. The identified ^{56}Ti nuclei are indicated. The right side of Fig. 1 shows the identification plot at the S4 focal plane of the FRS under the condition of ^{56}Ti identification at S2, clearly showing unreacted ^{56}Ti and the ^{55}Ti knockout residues.

3. Results and discussion

In this experiment we measured inclusive cross-sections and distributions of the parallel momentum of the knockout residues. In addition the detected gamma-rays allowed the selection of excited states populated in the knockout reaction and the determination of exclusive cross-sections and momentum distributions for those states. The measured data will be compared to theoretical calculations that are following Ref. [31] using the same elastic S-matrices for the computation of the single-particle cross sections and measured momentum distributions.

The theoretical single-nucleon removal cross sections have contributions from both the stripping mechanism (with excitation of the target by the removed nucleon) and the diffractive breakup mechanism. Following Ref. [32], these are computed from the residue- and nucleon-target eikonal S-matrices via the optical limit of Glauber theory. Computation of the elastic S-matrices used the point proton and neutron densities of the residues, taken from Skyrme (SkX) Hartree–Fock (HF) calculations [33]. The ^{9}Be density was assumed to be a Gaussian with a root mean squared (rms) radius of 2.36 fm. A zero-range forward scattering nucleon–nucleon (NN) amplitude was assumed with real-to-imaginary ratios interpolated from the table of Ray [34]. The rms radii of the removed nucleons' single-particle wave functions were also constrained by Skyrme (SkX) HF calculations, as is discussed in detail in [35]. Because of the insensitivity to bound state potential parameters noted there, we use a fixed diffuseness parameter $a_0 = 0.7$ fm and
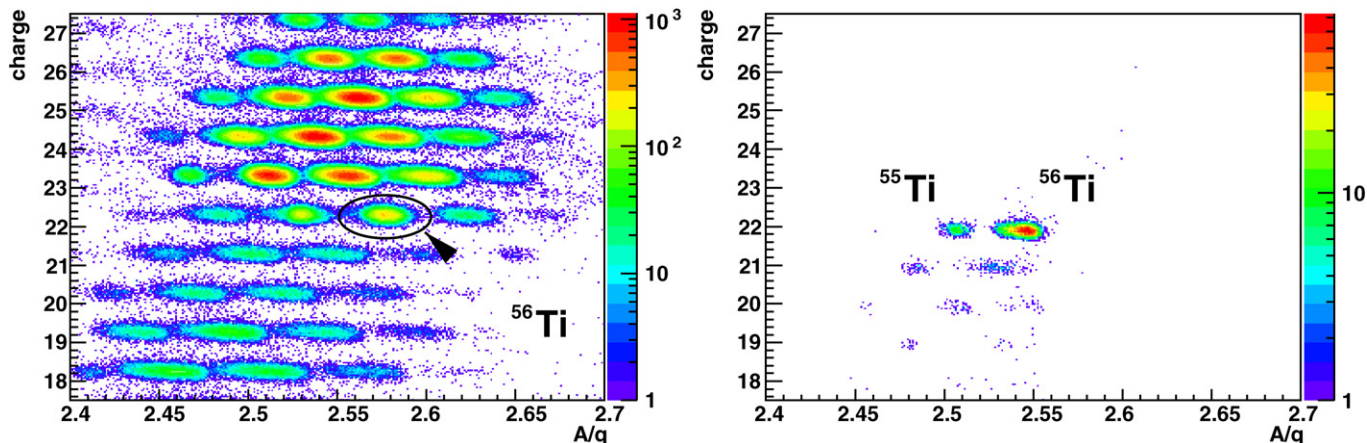
Fig. 1. (Color online.) *Left*: Charge vs. mass-to-charge ratio before the breakup target at the S2 focus of the FRS. *Right*: Charge vs. mass-to-charge ratio of fragments at the S4 focus of the FRS with ^{56}Ti identified at S2.

a spin–orbit interaction of 6 MeV for all cases. To compare with experiment the single-particle cross sections, calculated for unit spectroscopic strength, were multiplied by the shell model spectroscopic factors, which were calculated with Oxbash [36].

In the ^{48}Ca knockout experiment we measured an inclusive cross-section of 77(10) mb for the knockout to ^{47}Ca. The inclusive parallel momentum distribution of the identified ^{47}Ca residual nuclei is shown in the bottom left of Fig. 2 and compared to a fit that allowed for $L = 0$, $L = 2$ and $L = 3$ contributions, which are expected from the knockout of neutrons from the fully occupied $\nu s_{1/2}$, $\nu d_{3/2}$, and $\nu f_{7/2}$ orbitals. From the best fit individual contributions of 33(4) mb ($L = 3$), 23(3) mb ($L = 2$), 21(3) mb ($L = 0$) are extracted.

The gamma-ray spectrum observed in coincidence with identified ^{47}Ca residues is shown at the top of Fig. 2. The line at about 575 keV is a doublet of the 565 keV and 586 keV transitions from the well-known $3/2^+$ and $1/2^+$ states at 2578 keV and 2599 keV states in ^{47}Ca (see inlay). We have determined the FWHM resolution of MINIBALL after Doppler-correction to be 40 keV at this center-of-mass gamma-ray energy. The bottom right of Fig. 2 shows the exclusive momentum distribution in coincidence with both gamma-ray transitions after subtraction of events in coincidence with the background windows indicated in the gamma-ray spectrum. The exclusive cross-section for both excited states is 30(4) mb. The fit shown in the bottom right of Fig. 2 uses theoretical $L = 0$ and $L = 2$ components as expected for these states. On the basis of this fit, taking into account the known gamma-branching ratios for the decay of these states, we obtain individual cross-sections of 21(4) mb ($L = 2$) and 15(3) mb ($L = 0$) for the population of the $3/2^+$ and $1/2^+$ states, respectively. These cross-sections are within their uncertainties consistent with the results from the inclusive measurement. The relative cross-sections for all three states are within errors consistent with the expectations from shell model calculations while an overall reduction of about 0.65 of the spectroscopic factors is observed, which is the same reduction observed in (d, p) experiments [37] as well as knockout experiments at lower energy [35]. A more detailed discussion of the results from the ^{48}Ca knockout is given in Ref. [30].

The analysis of the ^{48}Ca reference experiment provides us with confidence on the understanding of the experimental set-up including all efficiencies and resolutions. With this we can turn to the main results on the knockout from ^{56}Ti to ^{55}Ti.

The bottom left panel of Fig. 3 shows the experimental inclusive longitudinal momentum distribution of all ^{55}Ti residues with a total cross-section of 83(12) mb. The relative strength of the theoretical $L = 1$ and $L = 3$ momentum distributions shown in the bottom left of Fig. 3 result from the shell model predictions using

the GXPF1A interaction. The theoretical inclusive cross-section of $\sigma_{\text{theo}} = 78$ mb is consistent with the measured value. It should be noted that the calculation predicts additional population of states just above the neutron separation energy with a cross section of 11 mb, which has not been included in the one-neutron removal cross section of 78 mb. However, while the GXPF1A predictions describe the inclusive cross-section and momentum distribution well, the data can also be described using the KB3G interaction (not shown), which predicts an inclusive cross-section of 74 mb. Thus the inclusive momentum distribution is not decisive concerning the question which interaction describes the structure of ^{55}Ti better.

Lets turn now to the top panel of Fig. 3 which shows the gamma-ray spectrum in coincidence with identified ^{55}Ti residues after Doppler correction. Only one statistically significant gamma-ray transition is observed at 955 keV, with 50 keV FWHM, consistent with the measured resolution from the ^{48}Ca experiment, and 48(12) counts above background. The hypothesis that there is only background in this region of the spectrum is consistent with the data only with less than 1% probability. We identify this transition with the depopulation of a new state at 955(6) keV in ^{55}Ti. The spectrum also shows an unresolved component up to high energies, indicating that other excited states have been populated as well.

The measured exclusive momentum distribution for the 955 keV transition is shown in the middle panel at the bottom of Fig. 3. Despite the low statistics the distribution is clearly consistent with $L = 1$ knockout, identifying this state as the $3/2^-$ state based on the $\nu p_{3/2}^{-1}$ single-hole configuration, which the GXPF1A calculations predict at about 1.2 MeV [19]. The observed cross-section for this state is $\sigma_{955} = 22(6)$ mb, which may include significant feeding contributions from higher-lying states. The theoretical prediction based on the GXPF1A interaction for the direct population of this state via $L = 1$ knock-out is 18 mb while a feeding of 9 mb from higher lying $3/2^-$ states is predicted. With the KB3G interaction the $3/2^-$ state is expected to lie at about 0.84 MeV excitation energy and should be directly populated with a cross-section of 35 mb with additional feeding contributions of 7 mb. Thus, the experimental cross-section is more consistent with the GXPF1A predictions.

The decisive distinction between the two SM predictions comes from their difference in the momentum distributions associated with knockout reactions populating the ^{55}Ti ground state. Since the direct population of the ground state in the reaction is not associated with gamma-ray emission, the ground state momentum distribution can in principle be extracted by subtracting the momentum distribution associated with all gamma-rays from the
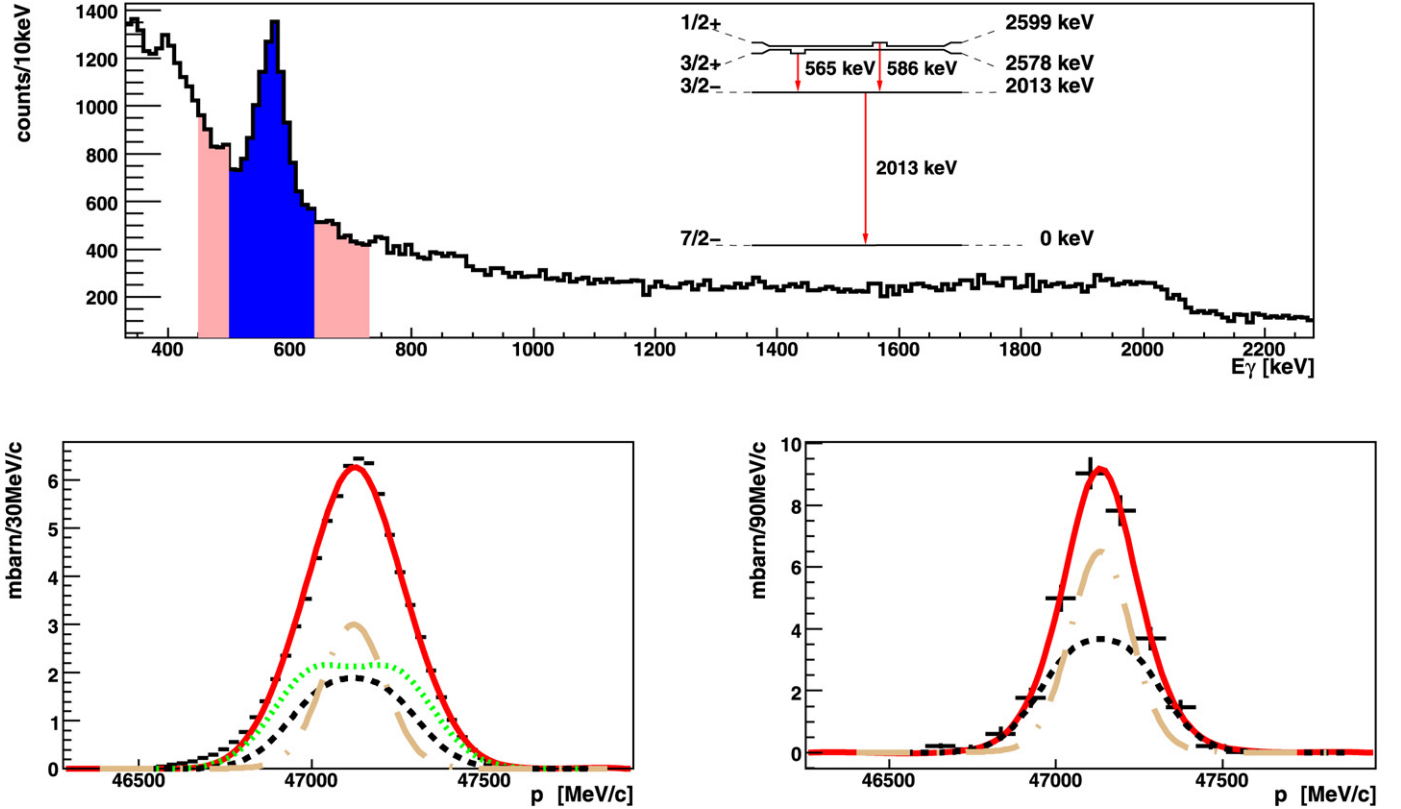
Fig. 2. (Color online.) *Top*: Doppler-corrected gamma-ray spectrum in coincidence with identified ^{47}Ca residues at S4. The inlay shows the relevant levels and transitions in ^{47}Ca. *Bottom left*: Inclusive momentum distribution for ^{47}Ca. The distribution was fitted with contributions from the $L = 0$ (long dashed dotted) $L = 2$ knock-out from $d_{3/2}$ (short dashed) and $L = 3$ $f_{7/2}$ (dotted) single-particle orbitals. The sum of the individual contributions is shown as solid line. *Bottom right*: Exclusive momentum distribution in coincidence with the two gamma transitions at 565 keV and 586 keV (unresolved in the gamma-ray spectrum) after background subtraction. The peak and background gates are indicated in the spectrum on top. The distribution was fitted with contributions from the $L = 0$ knock-out from $s_{1/2}$ (long dashed dotted) $L = 2$ knock-out from $d_{3/2}$ (short dashed). The sum of the individual contributions is shown as solid line.

inclusive momentum distribution for all ^{55}Ti residues. We will call this difference the *semi-exclusive momentum distribution for the ground state*.

However, in practice this procedure is not straightforward due to background from Bremsstrahlung photons as well as non-resolved gamma-transitions from all populated ^{55}Ti excited states. In addition, the analysis of events with no reaction in the target shows that at energies below 500 keV in the laboratory frame a background from Bremsstrahlung photons is dominant, while above 500 keV gamma-rays from the knock-out reaction prevail. Thus, only by considering gamma-rays above 500 keV in the laboratory frame, under the condition of an identified ^{55}Ti residue at S4, one can select gamma-rays from ^{55}Ti in a clean way. However, the gamma-ray spectrum contains, aside from the 955 keV photopeak, also a significant component combining unresolved photopeaks and Compton background of other states in ^{55}Ti. This continuous component with unknown contributions as well as the energy cut prevents an efficiency correction for the full gamma-ray spectrum. As a result we cannot determine the total cross-section for the momentum distribution in coincidence with all gamma rays. Therefore, we have to use an empirical scaling for the subtraction of the gamma-gated from the inclusive momentum distribution. We have chosen the scaling factor such that no negative values occur in the resulting semi-exclusive momentum distribution.

The resulting semi-exclusive momentum distribution is shown at the bottom right of Fig. 3. We claim that this semi-exclusive momentum distribution is representative of the ground-state momentum distribution as backed up by the analysis of simulated events discussed below. The extracted semi-exclusive momentum

distribution is well described by an $L = 1$ knockout while $L = 3$ knockout can be excluded, as shown by the theoretical curves in the bottom right of Fig. 3. This observation is consistent with the GXPF1A prediction that the ground state in ^{55}Ti has quantum numbers $J^{\pi} = 1/2^-$ based on the $p_{1/2}$ single-particle orbital. Contrary, the KB3G prediction would lead to a $5/2^-$ ground state and one would expect that the semi-exclusive momentum distribution would contain a dominant $L = 3$ component. Thus, the observed semi-exclusive momentum distribution provides clear evidence that the knockout to the ^{55}Ti ground state is of $L = 1$ character. This conclusion is not sensitive to the exact value of the scaling factor.

We performed simulations to investigate the significance of the extracted semi-exclusive momentum distribution. Using energies and transition matrix elements and spectroscopic factors from shell-model calculations on the basis of the GXPF1A and KB3G interactions, respectively, theoretical knock-out cross sections, momentum distributions, and gamma-ray transition intensities were calculated. These distributions were used to generate events for which GEANT4 [38] simulations of the experimental response of the MINIBALL/FRS set-up were carried out. Using these simulated events we extracted gamma-ray spectra and associated momentum distributions and applied the same analysis method as described above for the experimental data to obtain the semi-exclusive momentum distribution.

Fig. 4 shows as solid lines the semi-exclusive momentum distributions for the simulated events resulting from the subtraction of the gamma-gates ($E_{\gamma}^{\text{lab}} > 500$ keV) (dashed dotted lines) from the inclusive (dashed lines) momentum distribution. The former distribution was scaled in the case of the GXPF1A interaction (left)
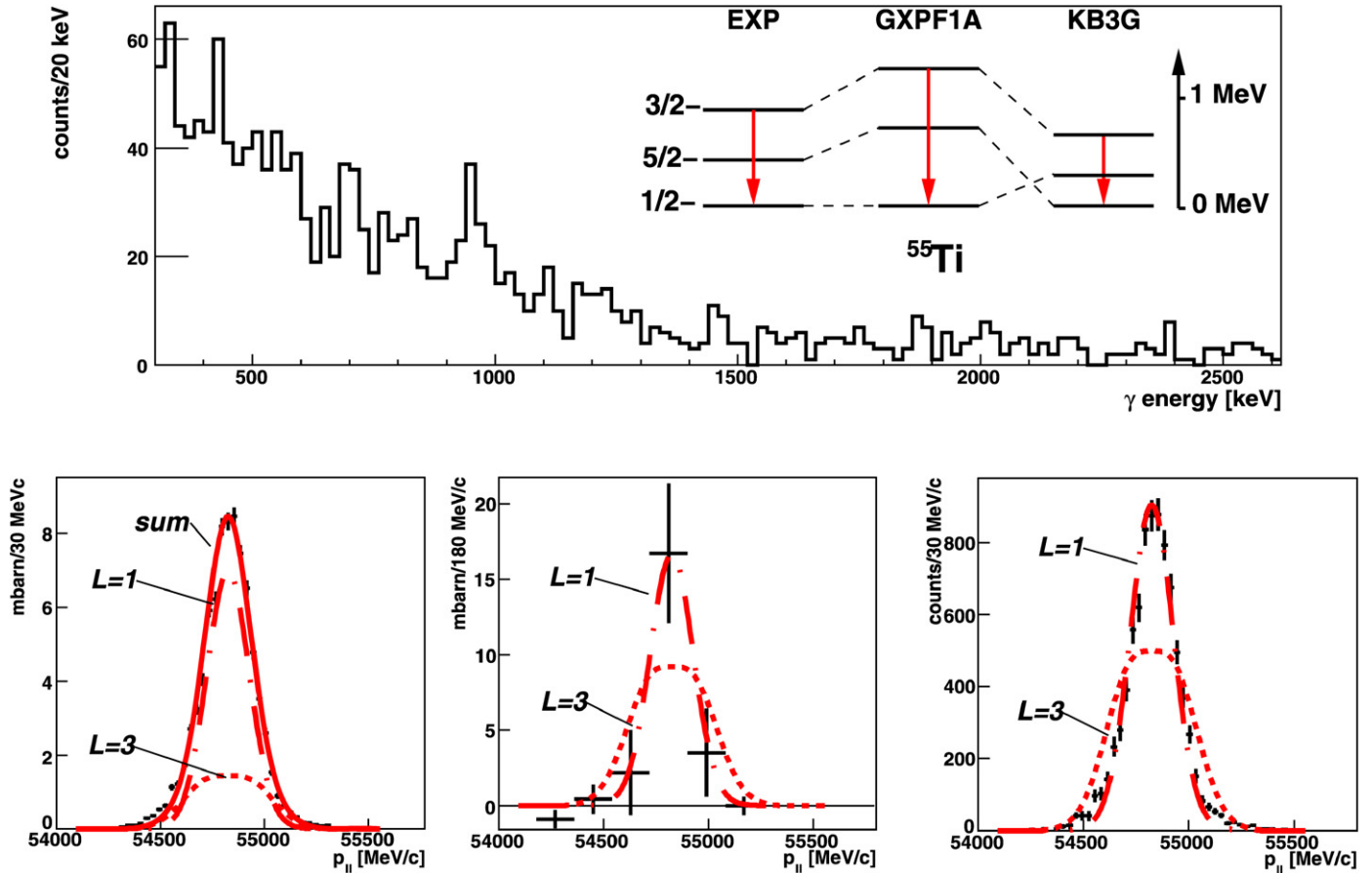
Fig. 3. *Top*: Doppler corrected measured gamma-ray spectrum for ^{55}Ti. Also shown are the lowest three experimental levels of ^{55}Ti together with SM predictions using the GXPF1A and KB3G interactions. *Bottom left*: Inclusive momentum distribution for ^{55}Ti in comparison with the predictions based on SM spectroscopic factors (solid line) using the GXPF1A interaction. Contributions for the $L = 1$ knock-out from $p_{1/2}$ (long dashed dotted) and $p_{3/2}$ (dashed dotted) as well as the $L = 3$ knock-out from $f_{5/2}$ (short dashed) and $f_{7/2}$ (long dashed) single-particle orbitals are shown. *Bottom middle*: Exclusive momentum distribution for the new 955 keV state in ^{55}Ti in comparison to theoretical predictions for $L = 1$ (dashed dotted) and $L = 3$ (dashed) knock-out. *Bottom right*: Semi-exclusive momentum distribution representing the ground state of ^{55}Ti, in comparison to theoretical distributions for pure $L = 1$ (dashed dotted) and $L = 3$ (dashed) knock-out (see text for details).
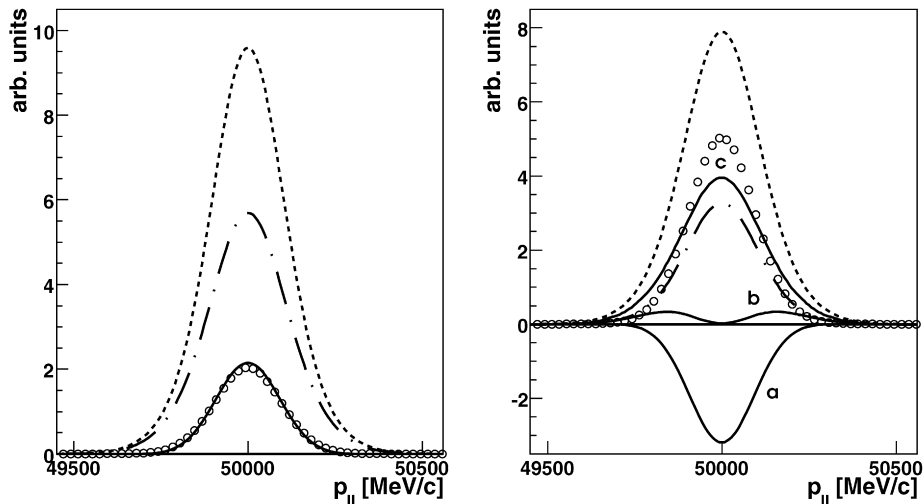

Fig. 4. *Left*: Simulated momentum distributions for ^{55}Ti based on SM calculations with GXPF1A: inclusive (dashed), gamma-gated with $E_\gamma^{\mathrm{lab}} > 500$ keV (dashed-dotted). The semi-exclusive momentum distribution (solid) resulting from the difference of both distributions is shown together with an $L = 1$ distribution (open circles), with a scaling similar to the choice made for the experimental distributions. *Right*: Same for SM calculations using the KB3G interaction. The difference of the two distributions is shown for three different scaling factors of the gamma-gated distribution with a scaling (a) similar as in the GXPF1A case, (b) to the height of the inclusive momentum distribution, and (c) to half the height of the inclusive momentum distribution.

such, that both distributions would be the same in the tails of the distribution, which corresponds to the choice made for the experimental data shown in Fig. 3. The resulting difference clearly agrees

with a pure theoretical $L = 1$ distribution (open circles). For the case of KB3G the difference is shown in the right panel of Fig. 4 for different scaling factors. There is no value of the scaling factor

that results in a semi-exclusive distribution that looks like a pure $L = 1$ distribution. For certain scaling factors a double humped distribution is observed as expected for the KB3G ground state with $L = 3$. Thus, these simulations clearly show that the observation of an $L = 1$ semi-exclusive momentum distribution is only consistent with a $1/2^-$ ground state of ^{55}Ti.

4. Summary

We have performed a relativistic one-neutron knockout experiment on ^{56}Ti using the GSI FRS as a two-stage magnetic spectrometer and the MINIBALL array for gamma-ray detection. Inclusive and exclusive cross sections and longitudinal momentum distributions were measured, allowing the determination of the orbital angular momentum of the populated states. We observed for the first time the 955(6) keV $3/2^- \nu p_{3/2}$ hole state in ^{55}Ti. The measured data for the first time establish the ground state of ^{55}Ti as $1/2^-$, in agreement with shell model predictions using the GXPF1A interaction and consistent with the tentative assignment of Ref. [19].

Acknowledgements

References

[1] O. Sorlin, M.-G. Porquet, Prog. Part. Nucl. Phys. 61 (2008) 602.
[2] T. Otsuka, et al., Phys. Rev. Lett. 87 (2001) 082502.
[3] T. Otsuka, et al., Phys. Rev. Lett. 95 (2005) 232502.
[4] T. Otsuka, et al., Phys. Rev. Lett. 97 (2006) 162501.
[5] N. Kaiser, W. Weise, Nucl. Phys. A 804 (2008) 60.
[6] M. Honma, et al., Phys. Rev. C 65 (2002) 061301.
[7] E.K. Warburton, et al., Phys. Rev. C 41 (1990) 1147.
[8] A. Poves, et al., Nucl. Phys. A 694 (2001) 157.
[9] E. Caurier, et al., Eur. Phys. J. A 15 (2002) 145.
[10] A. Poves, F. Nowacki, E. Caurier, Phys. Rev. C 72 (2005) 047302.
[11] T.R. Rodríguez, J.L. Egido, Phys. Rev. Lett. 99 (2007) 062501.
[12] A. Huck, et al., Phys. Rev. C 31 (1985) 2226.
[13] J.I. Prisciandaro, et al., Phys. Lett. B 510 (2001) 17.
[14] R.V.F. Janssens, et al., Phys. Lett. B 546 (2002) 55.
[15] P.F. Mantica, et al., Phys. Rev. C 67 (2003) 014311.
[16] S.N. Liddick, et al., Phys. Rev. C 70 (2004) 064303.
[17] B. Fornal, et al., Phys. Rev. C 70 (2004) 064304.
[18] B. Fornal, et al., Phys. Rev. C 72 (2005) 044315.
[19] S. Zhu, et al., Phys. Lett. B 650 (2007) 135.
[20] D.-C. Dinca, et al., Phys. Rev. C 71 (2005) 041302(R).
[21] A. Bürger, et al., Phys. Lett. B 622 (2005) 29.
[22] A. Gade, et al., Phys. Rev. C 74 (2006) 021302(R).
[23] A. Gade, et al., Phys. Rev. C 74 (2006) 047302.
[24] P. Adrich, et al., Phys. Rev. Lett. 95 (2005).
[25] A. Klimkiewicz, et al., Phys. Rev. C 76 (2007) 0516303(R).
[26] LAND Collaboration, in preparation.
[27] H. Geissel, et al., Nucl. Instrum. Methods B 70 (1992) 286.
[28] J. Eberth, et al., Prog. Part. Nucl. Phys. 46 (2001) 289.
[29] A. Bürger, Nucl. Instrum. Methods A 571 (2006) 739.
[30] P. Maierbeck, Dissertation, TU München, 2009.
[31] C.A. Bertulani, P.G. Hansen, Phys. Rev. C 70 (2004) 034609.
[32] P.G. Hansen, J.A. Tostevin, Annu. Rev. Nucl. Part. Sci. 53 (2003) 219.
[33] B.A. Brown, Phys. Rev. C 58 (1998) 220.
[34] L. Ray, Phys. Rev. C 20 (1979) 1857.
[35] A. Gade, et al., Phys. Rev. C 77 (2008) 044306.
[36] B.A. Brown, W.D.M. Rae, NuShellX, http://www.nscl.msu.edu/~brown/resources/resources.html, http://knollhouse.org.
[37] G.J. Kramer, H.P. Blok, L. Lapikás, Nucl. Phys. A 679 (2001) 267.
[38] http://geant4.cern.ch/.